ACS APPLIED NANO MATERIALS

Article

Zinc-Doped Mesoporous Graphitic Carbon Nitride for the Colorimetric Detection of Hydrogen Peroxide

Aftab Ahmed, Peter John, Mian Hasnain Nawaz, Akhtar Hayat, and Muhammad Nasir

ACS Appl. Nano Mater., **Just Accepted Manuscript** • DOI: 10.1021/acsanm.9b01036 • Publication Date (Web): 11 Jul 2019

Just Accepted

is published by the American Chemical Society. 1155 Sixteenth Street N.W., Washington, DC 20036

Zinc-Doped Mesoporous Graphitic Carbon Nitride for the Colorimetric Detection of Hydrogen Peroxide

Aftab Ahmed[1,2], Peter John[2], Mian Hasnain Nawaz[1], Akhtar Hayat[1*], Muhammad Nasir[1*]

[1] Interdisciplinary Research Centre in Biomedical Materials (IRCBM), COMSATS University Islamabad, Lahore Campus, 1.5 Km Defence Road, off Raiwind Road, Lahore, Punjab, Pakistan 54000

[2] Government College University Lahore, Katchery Road, Anarkali, Lahore, Punjab, Pakistan 54000

Highlights

- Development of a facile, highly sensitive, low cost, colorimetric detection method for H_2O_2 determination
- Zn doping was done in graphitic carbon nitride to increase its electrical properties for better sensitivity
- Structure and activity relationship were studied to better understand the high efficiency of the prepared catalyst

ABSTRACT: Recently, graphitic carbon nitride (g-C_3N_4) has been explored as a peroxidase-like catalyst for the non-enzymatic colorimetric detection of H_2O_2. In this study, we have developed a simple, low cost and eco-friendly hydrogen bond assisted soft template method of zinc ions doping in mesoporous graphitic-carbon-nitride (Zn-mpg-C_3N_4) thin nanosheets. Morphology and

composition of prepared samples were determined by different characterization techniques. PEG-1500 was beneficial to enhance the porosity and surface area of g-C_3N_4, whereas Zinc loading in the framework of g-C_3N_4 was resulted in the increase in electrical properties. The peroxidase-like catalytic activity of samples was investigated and compared based on the development of blue colored reaction mixture by the oxidation reaction between 3,3′,5,5′-tetramethylbenzidine and hydrogen peroxide (H_2O_2) through colorimetric method. The as-prepared 10% Zn-mpg-C_3N_4 has shown higher peroxidase-like activity as compared to natural HRP, g-C_3N_4 and mpg-C_3N_4. This enhanced peroxidase-like activity was attributed to the thin structured nanosheets, higher specific surface area, outstanding electron transfer ability, increased band gap and increased in charge separation of the catalyst through the direct zinc ions doping modification. The steady-state kinetics mechanism was investigated by using Michaelis-Menten Kinetics and found that the reaction followed Ping-Pong mechanism. This outstanding catalytic activity permitted us to design a rapid and convenient colorimetric sensing method to detect H_2O_2. Under the optimized condition, the developed sensor exhibited a linear range of 10 to 2000 μM (R-square = 0.9981), limit of detection as 1.4 μM and limit of quantification as 3.0 μM for H_2O_2 detection. In view of advantages compared with previous methods such as simple, facile operation, cost-effective, eco-friendly, naked eye observation and rapid response, the developed sensor possesses huge potential and a promising candidate for enzyme mimic sensing of H_2O_2 in the environmental as well as in the biological samples.

KEYWORDS: Graphitic Carbon Nitride; Zn doping; Peroxidase-like activity; Hydrogen Peroxide; Colorimetric detection.

1. INTRODUCTION

The powerful oxidizing behavior of hydrogen peroxide (H_2O_2) has made its critical in many fields such as in chemical, biological and clinical fields. Therefore, it is of vital importance to monitor its level for various applications.[1] Different analytical techniques are used for the detection of H_2O_2 such as those based on colorimetric,[2-3] electrochemical,[4] photoelectrochemical,[5] chemiluminescence,[6] and fluorescence detection methods. The colorimetric method of detection is low cost, simple and practical. This method is easy in terms of monitoring the progress of reaction by naked eye and does not require any expensive instrument or skilled operator. The initial assay by this method was performed using natural enzymes as catalyst to convert substrate into an optical colored product. Despite high selectivity and specificity, natural enzymes undergo drawbacks such as instability and denaturing phenomena, which have made enzymes unsuitable for sensing applications.[7]

Nanoparticles have small size, large surface area, and controlled catalytic potential.[8] Some nanoparticles exhibited enzyme like activities and applications of these enzyme-mimic-activities in various fields are remained hot research area.[9] Such nanoparticles-based artificial enzymes are referred as nanozymes.[10] They are supposed as alternative to natural enzymes and are exploited to catalyze H_2O_2 reactions.[11] They have low cost, facile synthesis, high stability and easily to manipulate in the field of optical sensing.[12] Different kinds of nanozymes such as carbon based, metallic,[13] metal oxides,[14-15] and metal oxide nanocomposites[16] have been employed to replace natural enzymes. Porous type nanomaterials are formed by interconnecting of large mesopores with surface and structural defects has also shown enzyme like activities.[17] The quest for abundant, inexpensive, metal free, fascinated and tunable electronic structured nanomaterial's having specificity, chemical and thermal stability are remained focused area in this area of research.[18-19]

Carbon-based nanomaterials are low cost, easily available, thermally and chemically stable, environmentally friendly and easy to large-scale production. In present colorimetric assay, among carbon-based nanomaterials, graphitic-carbon-nitride (g-C_3N_4) was used for the development of carbon-based biomimetic sensor. It is an organic semiconductor with band gap of 2.7 eV. Its structure is analogous to graphitic structure, which imparts special optical features in it. However, due to some intrinsic defects in g-C_3N_4 such as high recombination percentage of photo generated charge carriers[20] and low electron transfer ability, imparts special challenges in its use for sensing applications. To solve these limitations, various approaches such as doping, nano-structuring using soft / hard templates, surface modifications, construction of heterostructures or nanocomposites have been proposed.[21] These modifications have improved its properties[22] and enhanced its applications in various fields like sensing and biosensing.[23] Among these modifications, the use of additive for preparation of porous ultrathin nanosheets along with elemental binding / doping for tuning the structure and reactivity[24-25] have built up a novel way to fabricate g-C_3N_4 base functional nanostructures and are becoming a hot research topic. It is expected that peroxidase-like activity of sample would be improved greatly by these modifications. In past, soft templates like ammonium chloride or thermal treatments was used to obtain different nano-structures of g-C_3N_4 such as exfoliated nanosheets, wrinkled nanosheets, nano-horned and worm shaped products with porosity. However, the choice of templates, which are environmentally friendly and give high yield in a simple and single step to safe time are remained under study.

Polyethylene glycol (PEG) can act as a model structure directing template because of its low cost, low toxicity, relative stability, environmental friendliness, and uniform and well-ordered chain structure. Its ether oxygen forms week hydrogen bonds with melamine that could be exploited to prepare a controlled, well-structured and self-assembled porous thin nanosheets.[26]

Thermal condensation of melamine began in the range of 300 - 350°C, whereas PEG oxidized and decomposed to carbonaceous gases at 480°C. PEG and carbonaceous gases may prevents the complete staking of g-C_3N_4 intermediates compounds, which may result in the formation of porous thin sheets of g-C_3N_4.

The inclusion of transition metals and some rare earth metals in g-C_3N_4 was reported earlier to improve its catalytic properties by improving surface area, electron transferability and porosity.[27] These metals inclusions were considered due to the availability of six electrons of nitrogen atoms in each triangle of g-C_3N_4 structure. The incorporated metallic species in the structure of g-C_3N_4 semiconductor can dope electrons to such semiconductors.[28] Transition metals like iron, cobalt and copper ions doped g-C_3N_4 nanostructures has shown better peroxidase-like catalytic activity. However, alkali-metal or transition metal-doped g-C_3N_4 cater some disadvantages, for example, the thermal stability of the doped ions is poor as they run off particularly easily into the aqueous solution by proton interaction and relatively weak bonding with the adjacent carbon nitride layers. Furthermore, the newly created energy bands might act as recombination centers, leading to decreased quantum efficiencies.[27] Compared with different doped metals, Zinc (Zn) incorporation in the graphitic framework of g-C_3N_4 is easier as a result of the interaction between positively changed zinc and negatively charged nitrogen and it does not destroy the basic graphitic framework at lower concentrations.[29] Zn doping is also advantageous, as it creates a tighter covalent interaction with the nitrogen atoms by contributing the 4s electrons. The incorporated Zn species capture the photo generated electrons from the conduction band and accelerate the charge transfer and inhibit the recombination of electron-hole pairs. This results in the enhancement of electron-hole transfer between g-C_3N_4 and Zn. Due to this unique charge distribution and extended π-conjugated system by Zn dopant, more active sites are created for

TMB oxidation.[30] Therefore, additive hydrogen bonded assisted method and metallic elemental doping were considered more feasible techniques to design especial porous nano-structures of the product. It was also supposed that these preparation techniques may alter size, band gap, electrical properties and photochemical properties of g-C_3N_4, which may cause enhancement of the peroxidase-like activity of the catalyst.

Herein, we have successfully prepared and demonstrated zinc (Zn) doping in mesoporous g-C_3N_4 using PEG-1500 as a soft template as shown in Scheme 1. The synergistic effect of Zn doped samples was investigated and described in detail. Peroxidase-like activities of Zn doped mpg-C_3N_4 nanosheets were enhanced for detection of H_2O_2. We have also investigated the catalytic kinetics and optimized product reaction mechanism. By using peroxidase-like activity of thin nanosheets of the catalyst, a cheap and green colorimetric method for the H_2O_2 detection was developed.

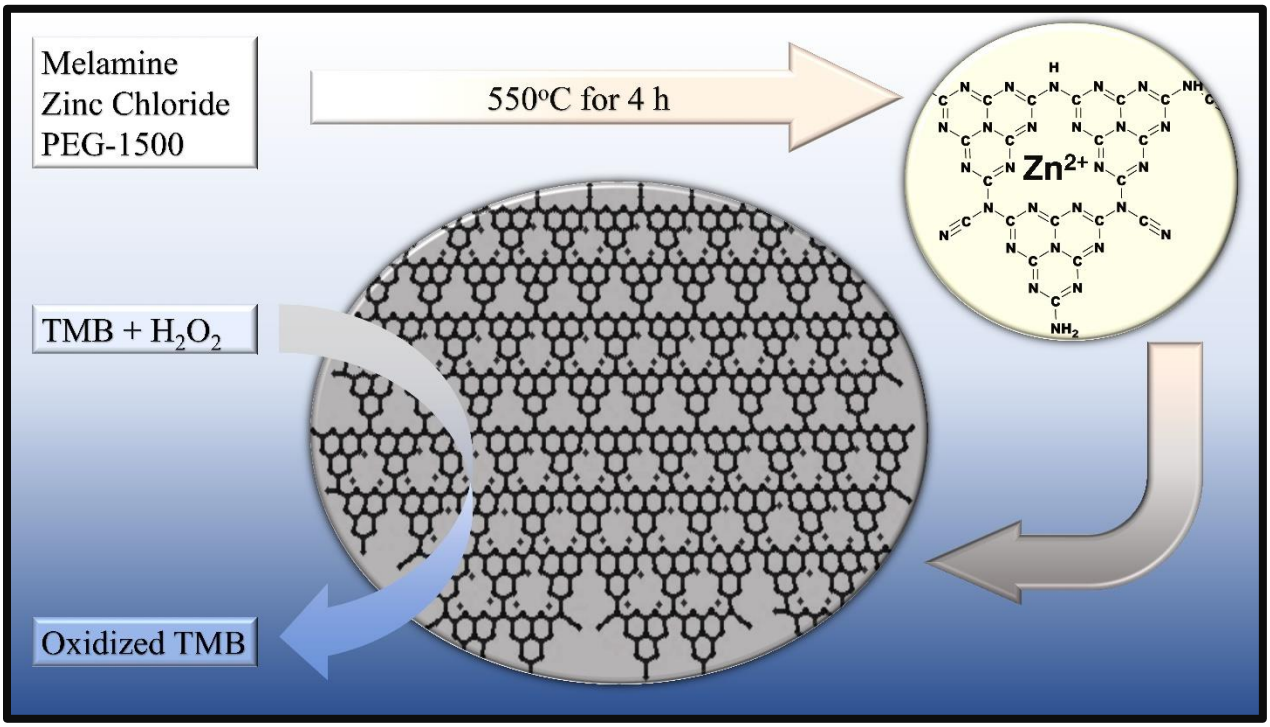

Scheme 1. Systematic representation of proposed mechanism for the colorimetric detection of H_2O_2 by TMB and Zn doped mpg-C_3N_4 nanosheets.

2. EXPERIMENTATION

2.1 Reagents and Materials

Melamine was received from Analar. Acetic acid, zinc chloride dihydrated ($ZnCl_2$•$2H_2O$) and TMB were received from Sigma Aldrich. Sodium acetate anhydrous was obtained from Daejung. H_2O_2 (30%) was obtained from Merck KGaA. Polyethylene glycol 1500 (PEG-1500) was received from Panreac. Dimethyl sulfoxide (DMSO) was received from Lab Scan. Hydrochloric acid solution was obtained from BDH. Sodium hydroxide pellets was received from Omicron. All chemicals were of analytical standard, used as received. All solutions were made by deionized water obtained from an Elga-Pure-LAB@Ultra deionizer.

2.2 Characterizations

X-ray diffraction (XRD) analysis was performed on Rigaku-D/max-2500-PC diffractometer with a graphite typed monochromator (40kV, 40mA). Nickel filtered Cu-Kα radiations having wavelength of 1.5418Å was used during the analysis. Surface morphology and shape were obtained using Vega 3, LMU, Tescan scanning-electron-microscope (SEM). SEM images were obtained at 10kV. Elemental analysis as well as purity were determined by using energy-dispersive X-rays spectrometer (EDX) on same SEM device. Double adhesive tape supported gold coated samples were mounted on aluminum support for analysis. Morphologies and microstructure of the samples were determined through transmission electron microscopy (TEM) and measurements were carried out on a transmission electron microscope (JEM-2010F, JEOL, Japan) with an acceleration voltage of 200 kV. The Brunauer-Emmett-Teller (BET) specific

surface area, pore sizes distribution and pore volume were measured BET method. The BET and Barrett-Joyner-Halenda (BJH) measurements were carried out by using Micrometrics ASAP 2020 (V 4.00 H) surface area / porosity analyzer. X-ray photoelectron spectroscopy (XPS) was used to determine the chemical environment and chemical state of the elements present in the samples. XPS measurements were carried on Axis Ultra spectrometer system with a mono-chromatized Aluminum-Kα X-ray radiation source (225 W). The high resolution XPS spectra were recorded for carbon (C) 1s, nitrogen (N) 1s and Zn 2p regions. For functional groups determination, Fourier-transform-infrared (FTIR) spectra were scanned in absorption manner in wavenumber range of 670 - 4000 cm^{-1} using Thermo-Fisher-Scientific (Nicolet, 6700) spectrophotometer, a resolution of 8 cm^{-1} in attenuated total reflectance (ATR) mode at room temperature, using one scan per spectrum. For estimation of band gap, ultra-violet-visible (UV-Vis) diffuse-reflectance-spectra (DRS) were scanned on Perkin-Elmer-Lambda 35 spectrophotometer. Barium sulphate was standard reference and samples were pressed into thin tablet under ambient temperature conditions. Absorption edge was used for band gap calculation. In colorimetric analysis, to find wavelength of maximum absorption (λ_{max}) and change of absorption peak intensity of reaction system, UV-Vis absorption spectra of reaction system were noted using Perkin-Elmer-Lambda 25 UV-Vis double beam spectrophotometer (UV-25, Perkin Singapore) with quartz cuvette capacity of 3 mL and bandwidth setting (1 nm) at a wavelength scan rate of 960 nm min^{-1} in wavelength range 400 - 800 nm. Raman and photoluminescence spectra of samples were recorded using InVia-laser-scanning-confocal-microscope (Reni Shaw, UK) at 457 nm laser excitation wavelength. The laser exposure time was set at 10s with grating, objective and laser power of 1800 I min^{-1}, 5x, and 0.1% respectively.

2.3 Synthesis of Zn-mpg-C_3N_4

The preparation of Zn doped mesoporous-graphitic-carbon-nitride (Zn-mpg-C_3N_4) was done by calcination technique with minor modifications as reported earlier.[31] Briefly, 11.1 g of melamine and 2.3 g of PEG-1500 were mixed in 50 mL of the ethanol containing $ZnCl_2$•$2H_2O$ solution. The resultant suspension was heated at 80°C with continuous stirring for removal of ethanol to form a white solid. Fine grounded white solid was transferred into ceramic boats, heated under static air at temperature ramp of 5°C min^{-1} to achieve final temperature of 550°C and held at 550°C for 4 h. After completion of reaction, the product was cooled under normal conditions. As a result, a pale-yellow product was obtained, which was mechanically ground to fine powder in pestle mortar and used for checking of peroxidase-activity. Various samples were prepared by varying amount of $ZnCl_2$•$2H_2O$ (0, 0.005, 0.012, 0.019, 0.027, 0.0578, 0.111, 0.333 and 0.555 g) and wt. percentage of Zn with respect to product amount was calculated (0, 1, 2.2, 3.3, 4.7, 10, 15, 38 and 52). The resultant samples were labelled as wt. % of Zn-mpg-C_3N_4. The g-C_3N_4 was synthesized without the addition of PEG-1500 and $ZnCl_2$•$2H_2O$ under the same reaction conditions.

2.4 Peroxidase-like Catalytic Activity and Steady-State Catalytic Kinetics Assay

To examine and compare peroxidase-like activity, two-dimensional nanostructures having thickness ranging from 1 to 100 nm called as nanosheets were prepared and used for reaction between TMB and H_2O_2. Stock suspension (2.7 mg mL^{-1}) of each sample in distilled water was prepared by ultrasonication with R60% at 60°C for 30 min. This suspension (75 µL) was separately added into sodium acetate buffer (2820 µL, 100 mM, and pH 4) and mixed well. Then, 45 µL of TMB (stock 20 mM in DMSO) and 60 µL of H_2O_2 (stock 20 mM in dist. water) were added in reaction mixture. Final concentration was 68 µg mL^{-1}, 300 µM and 400 µM for nanosheets, TMB and H_2O_2 respectively. Reaction mixture turned blue due to the oxidized TMB and a prominent

absorption peak at 652 nm (A_{652} nm) in the UV-Vis absorption spectrum was observed. Such reaction are dependent on the amount of nanosheets, so measurements were carried out by controlling the amount of nanosheets suspension in the reaction mixture. Peroxidase-like activity depends upon the pH of buffer, temperature, catalyst concentration and substrate (TMB, H_2O_2) concentration, therefore catalytic measurements were carried by varying pH (2.0 - 6.0), temperature (20 - 40^oC), amount of catalyst suspension (0 - 100 µg mL^{-1}), TMB concentration ([TMB], 0 - 620 µM) and H_2O_2 concentration ([H_2O_2], 0 - 16 mM) in 100 mM acetate buffer.

Kinetics studies were performed by determining the A_{652} nm with respect to reaction time. Biomimetic determinations for mechanism study were performed by varying [H_2O_2] at fixed [TMB] or vice versa. Steady-state dynamics kinetics constant parameters (K_m and V_{max}) were calculated from the initial linear ranges of the initial reaction rates of kinetics curves by Line-weaver-Burk plots (1 / velocity against 1 / [substrate]) of the double reciprocal of Michaelis-Menten-equation, [$V = (V_{maximal} \times [S]) / (K_m + [S])$]. Where, V and $V_{maximal}$ were velocities of the reaction, K_m was Michaelis-Menten constant and [S] was the concentration of the substrate.

3. RESULTS AND DISCUSSION

To find out the structural morphology, SEM images of prepared samples were obtained as seen in Figure 1. The g-C_3N_4 was hierarchical platelet type analogous to the graphite, while micron sized g-C_3N_4 was stacked. It was obvious that after introduction of PEG-1500 as soft template in the synthesis process, mpg-C_3N_4 has displayed stacked typed morphology with several hundred nanometers sized chips. This revealed that PEG-1500 was beneficial to increase the number of small pores on the surface. Moreover, after $ZnCl_2$•$2H_2O$ addition along with PEG-1500 in melamine and the resultant mixture calcination (550^oC, 4 h), the SEM image of 10% Zn-mpg-C_3N_4 has showed that pores were blocked with Zn loading.

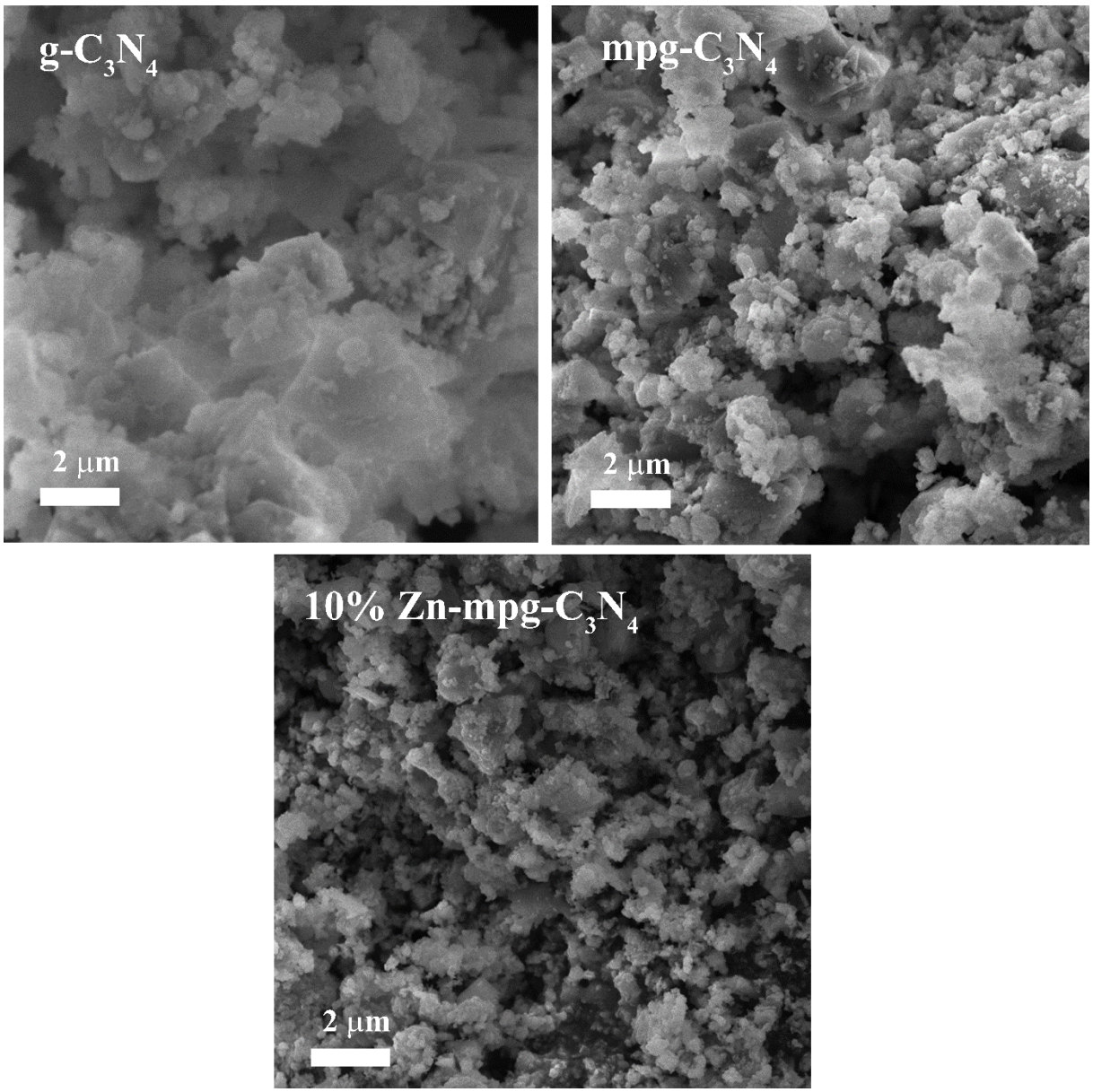

Figure 1. SEM images of prepared g-C_3N_4 based modified samples.

EDX images of the prepared samples are presented in Figure S1. EDX labelled peaks in g-C_3N_4 as well as in mpg-C_3N_4 were corresponding to C and N atoms, whereas in 10% Zn-mpg-C_3N_4 were corresponding to C, N and Zn atoms. Some other peaks were corresponding to elements

used for sputter coating for EDX analysis. Table 1 represented the comparison of elemental percentages.

Table 1. Comparison of g-C_3N_4, mpg-C_3N_4, and 10% Zn-mpg-C_3N_4 EDX elemental analysis.

Samples	Wt. %Zn	Wt. %N	Wt. %C	Atomic %Zn	Atomic %N	Atomic %C
g-C_3N_4	-	49	51	-	46	54
mpg-C_3N_4	-	58	42	-	54	46
10% Zn-mpg-C_3N_4	28	27	45	7	32	62

EDX results supported the presence of N and C atoms in g-C_3N_4 as well as in mpg-C_3N_4 whereas Zn, N and C atoms in 10% Zn-mpg-C_3N_4. However, higher percentage of C atoms was due to the involvement of C atoms form laser light and from double adhesive tape.

To determine the specific surface areas, porosity and pore-size-distribution of prepared samples, nitrogen adsorption-desorption isotherms were obtained. Figure 2 showed that all the samples exhibited type IV adsorption isotherms according to Brunauer-Deming-Deming-Teller (BDDT) classification system. The amount of nitrogen gas adsorbed for 10% Zn-mpg-C_3N_4 was much larger than the amount of nitrogen gas for g-C_3N_4, which indicated the formation of enlarged mesopores. According to the International Union of Pure and Applied Chemistry (IUPAC) guideline, H3 type hysteresis loop was observed in the range from 0.65-1.0 P/P_o for 10% Zn-mpg-C_3N_4, which also indicated the mesoporous features in the sample. These mesopores was originated from the stacking of g-C_3N_4 nanosheets since the PEG-1500 and doped Zn species strongly effected the interlayers packing of g-C_3N_4 nanosheets through N-bridge linking. Such effect was resulted in an increase of space between the interlayers. The BET surface area of 10% Zn-mpg-C_3N_4 was determined as 9.8 m^2/g, which was about 3.6 times of the g-C_3N_4 (2.8 m^2/g).

This enhancement in surface area was ascribed to the generation of mesoporous structure, reduction of thickness and size of the mpg-C_3N_4 layer. Furthermore, the pore-size-distribution was also determined from the adsorption branches of the isotherms by using BJH method as shown in insert of Figure 2. The BJH adsorption pore diameter for g-C_3N_4 and 10% Zn-mpg-C_3N_4 was calculated as 80.4 and 18.8 nm, whereas adsorption cumulative volume of pores was calculated as 0.014 and 0.029 cm^3/g respectively. These finding revealed that the pores in 10% Zn-mpg-C_3N_4 were corresponding to the mesoporous structure. The BET average pore width of 10% Zn-mpg-C_3N_4 (12.4 nm) exhibited a quite broad pore-size-distribution (2 - 90 nm) with small mesopores (2.5 and 4.6 nm) and large mesopores (31.1 nm), which further confirmed the generation of more mesopores in the 10% Zn-mpg-C_3N_4. The small mesopores were produced due to the porosity in nanosheets created by soft template and Zn-N interaction due to the splitting of the large layers during the synthesis process. The large mesopores were formed by the packing of g-C_3N_4 layers. Therefore, the introduction of mesoporosity into g-C_3N_4 has enlarged the surface area and decreased the pore volume, which were beneficial in providing more possible redox reaction active sites. Thus, this work showed that 10% Zn-mpg-C_3N_4 with enhanced porous surface areas can be prepared by using soft template like PEG-1500.

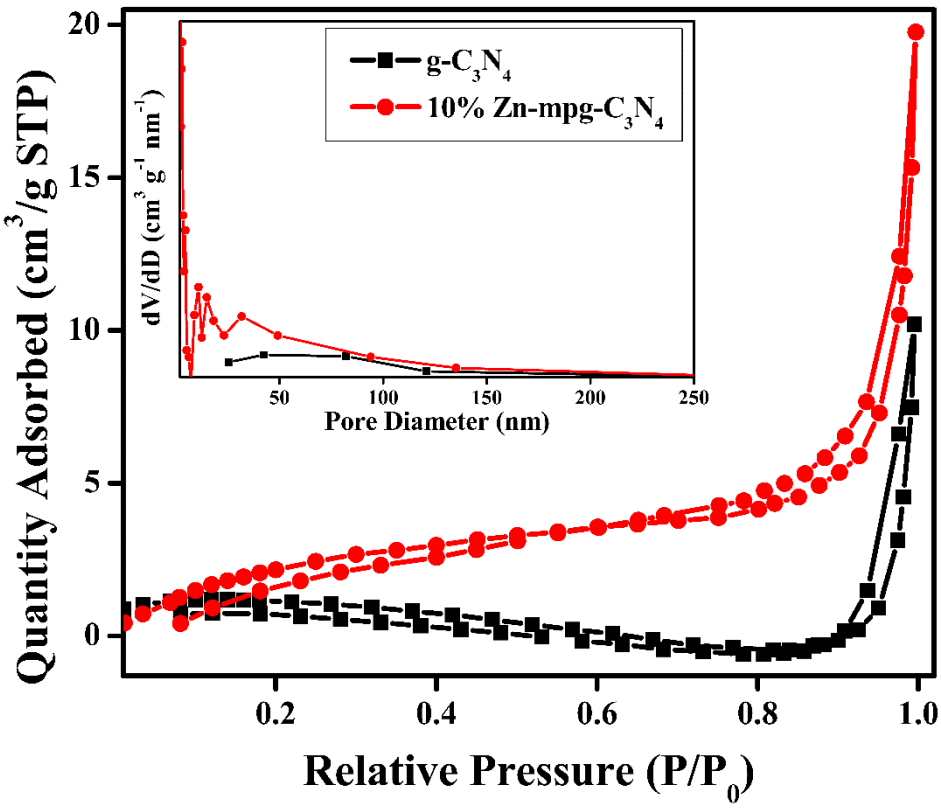

Figure 2. Nitrogen adsorption-desorption isotherms and corresponding BJH pore size distribution curves (inset) of the samples.

The morphologies and microstructure of g-C_3N_4 and Zn-doped mpg-C_3N_4 samples were investigated via TEM. Figure 3A showed the TEM image of g-C_3N_4. It can be clearly seen that aggregate of free-standing nanosheets with edges tended to be ragged to minimize their surface area. A dense and stacked architecture was obtained. Figure 3B and Figure 3C showed the low-resolution and high-resolution TEM images of 10% Zn-mpg-C_3N_4. High-resolution image showed the mesoporous structure consisting of irregular, wrinkled and small flat sheets. Many pores with mean diameter of 10 - 45 nm were distributed on the sheets. Furthermore, this pore size was much greater than the size of Zn^{2+} (~74 pm). The presence of somewhat transparency indicated that sample was made of few atomic layers with mesoporous structure, but low-resolution image

supported the presence of Zn in the porous structure. It is speculated that PEG-1500 proceeded to the crystal lattice during the formation of mpg-C_3N_4, which may be changed its morphology. Considering above observations, it can also be concluded that the 10% Zn-mpg-C_3N_4 sample was more fragmental, thin and smaller with mesoporous structures as compared to earlier reported samples. Meanwhile, Zn element and its oxides forms were not found in TEM image, which representing that the state of Zn in 10% Zn-mpg-C_3N_4 sample was ionic. The thin nanosheets with porous structure resulted in the increase of surface to volume ratio and reactive site numbers, which can enhance the peroxidase-like catalytic activity of Zn-mpg-C_3N_4.

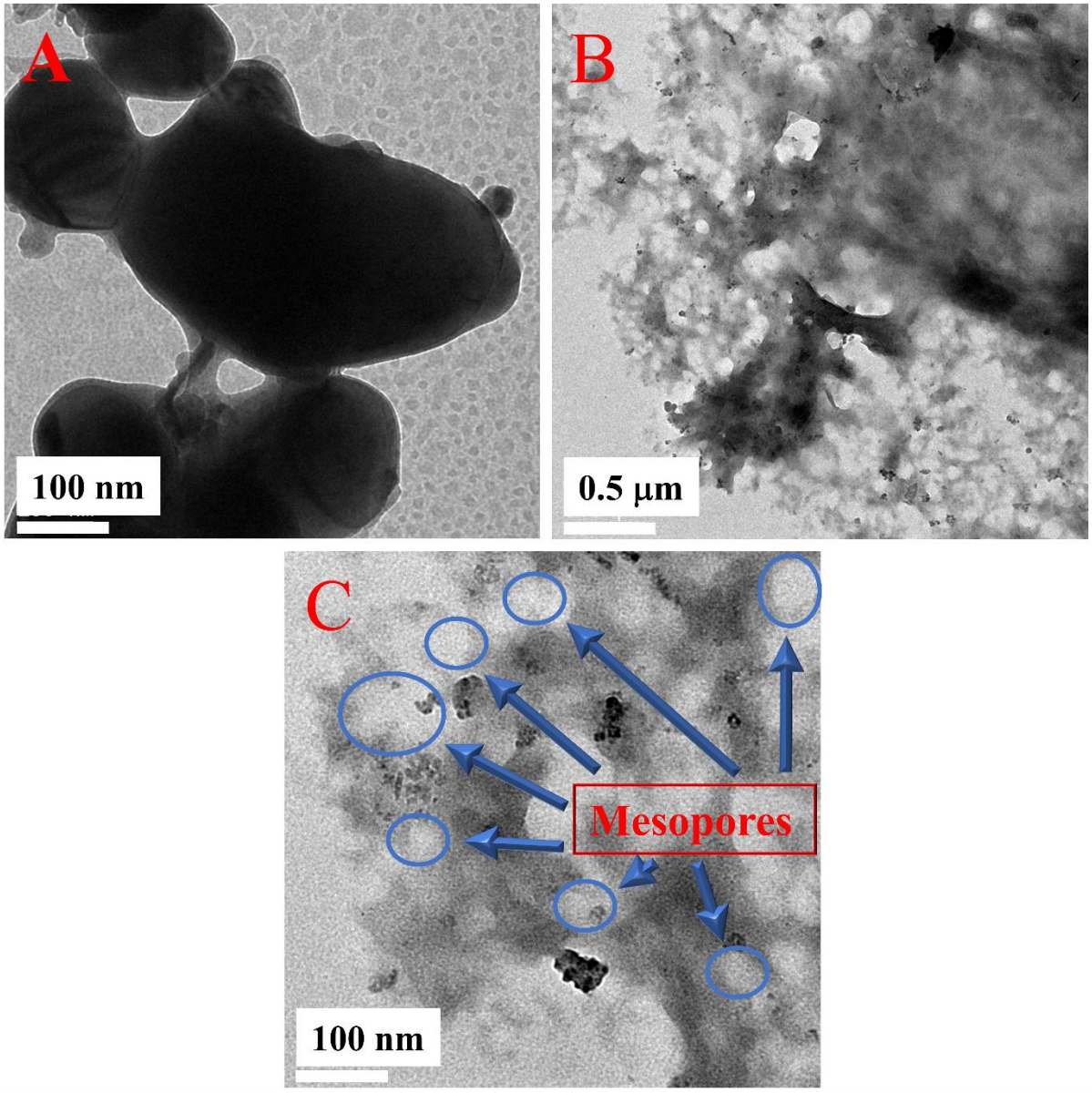

Figure 3. TEM images of g-C_3N_4 (A) and 10% Zn-mpg-C_3N_4 (B and C).

As can be seen in Figure 4, XRD patterns confirmed the presence of graphitic like structure in all the samples. Diffraction peaks in spectra was corresponding to the structure of g-C_3N_4. A minor diffraction peak around 15.8^o in the spectra of g-C_3N_4, mpg-C_3N_4 and 10% Zn-mpg-C_3N_4 were corresponding to index (100) planes with interplanar distance of 0.55 nm was arising from the in-planar structural packing motifs. Intensity of this peak was decreased in the case of mpg-

C_3N_4 and Zn-mpg-C_3N_4. Similarly, a major peak in the spectra of g-C_3N_4 and mpg-C_3N_4 was observed around 26.5° corresponding to index (002) planes with interplanar distance of 0.336 nm arising from the typical interplanar stacking of hexagonal g-C_3N_4 (JCPDS-PDF 01-087-1526) (JCPS-PDF 01-087-1522).[32] A decrease in intensity of major peak in mpg-C_3N_4 spectra indicated the presence of thin and porous structure in mpg-C_3N_4 nanosheets. However, in the case of 10% Zn-mpg-C_3N_4 spectra, this peak was slight shifted and further decrease in peak intensity was observed. In addition of (100) and (002) indexed planes, a small variation in intensity and small shift in 2θ of indexed planes (001), (201), (102), (111), (300), (220), (302) and (203) in XRD patterns of 10% Zn-mpg-C_3N_4 were observed as compared to that of the g-C_3N_4 and mpg-C_3N_4 XRD patterns. These variations were due to decrease in crystallinity, generation of edge defects and zinc ion doping in the thin and porous structure of mpg-C_3N_4. There was no diffraction peak observed corresponding to Zn or ZnO phase in the samples, which also indicated that Zn metal ions were chemically coordinated / embedded in host graphitic structured planes possibly in the form of Zn-N coordination bonds. Therefore, introduction of PEG-1500 and external Zn ion doping treatment during calcination process alleviated the crystallinity and generated porosity in the samples.[25, 28]

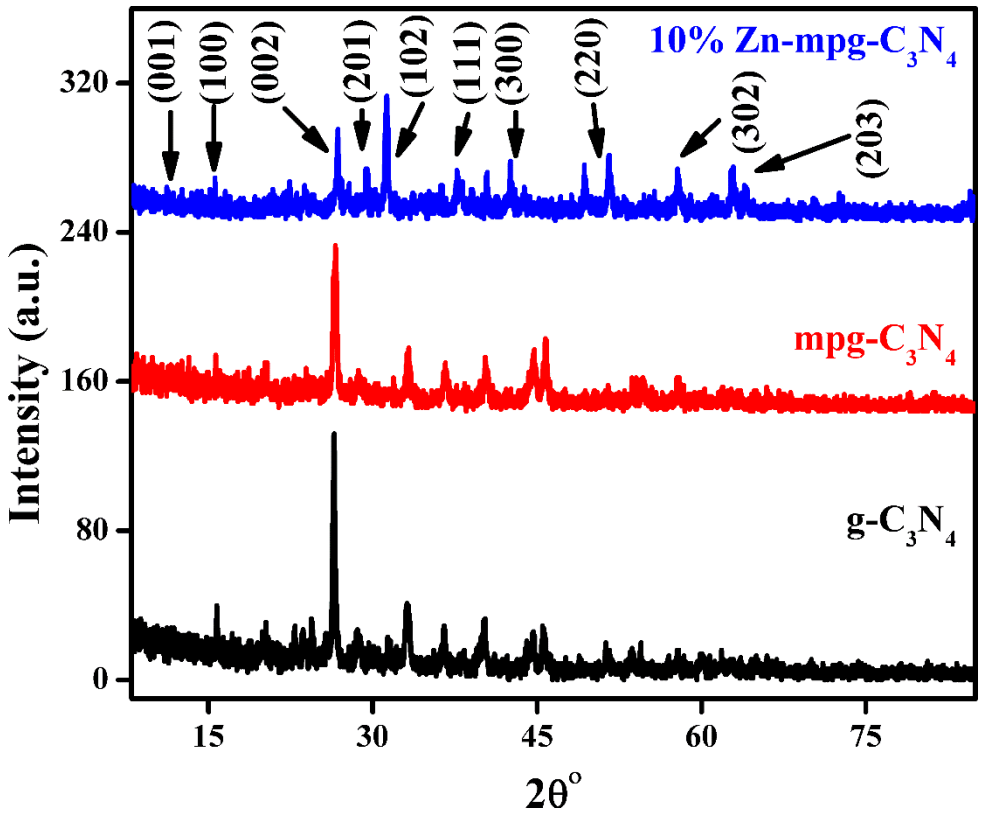

Figure 4. XRD analysis of g-C_3N_4, mpg-C_3N_4 and 10% Zn-mpg-C_3N_4.

XPS measurements of the samples were carried out to determine the chemical environment and chemical state of the elements (C, N and Zn). Surface probing technique was used to determine the local structure of g-C_3N_4 and metallic nature of Zn. Figure 5 showed the high resolution XPS spectra of C, N and Zn elements in the prepared samples. High resolution C 1s XPS spectra in Figure 5A showed the presence of mainly three different Gaussians-Lorentzian peaks upon deconvolution. The C 1s peak at binding energy of 284.5 eV was ascribed to the graphitic or amorphous C atoms from instrument and surface adsorbed adventitious hydrocarbons in purely carbonaceous environment containing C-C coordination and determined as standard C. The C 1s peaks at 287.6 and 288.3 eV was ascribed to sp^2-hybridized C atoms in aromatic ring bonding with $-NH_2$ group, sp^3-hybridized C atoms ($C-(N)_3$) and sp^2-hybridized C atoms attached to the N in

aromatic ring as N-C=N to form a pure graphitic site in a C-N-C coordination. Figure 5B showed N 1s high resolution XPS spectra. N 1s peak were deconvoluted into four different peaks with binding energies centered at 398.6, 400.1, 401.2 and 404.5 eV. The main dominant peaks at 398.6 eV and 400.1 eV were attributed to sp^2 hybridized N atoms in C-N=C group of triazine ring and to the tertiary N atoms in N-$(C)_3$ group, which connecting C_6N_7 structural motif. The peaks at 401.2 eV and 404.5 eV were corresponded to N atoms with ≡N and -N- bonding and charge effect, respectively. Deconvoluted high resolution XPS spectra of Zn 2p and Zn LMM Auger region of samples are shown in Figure 5C. A doublet in Zn 2p spectrum was appeared with binding energies located at 1044.9 and 1021.8 eV, assigned to Zn $2p_{1/2}$ and Zn $2p_{3/2}$ lines respectively. The difference of binding energies between these peaks is 23.1 eV, which indicated that Zn ions in the sample were of a +2 oxidation states. Further, binding energy of Zn $2p_{3/2}$ peak was lower than binding energy of $ZnCl_2$ (1021.9 eV). The presence of peak at 496.5 eV in Zn LMM Auger spectrum confirmed the existence of Zn-N bonds. The Zn-N bonds helped in charge transfer from guest Zn to the host g-C_3N_4, which was important for enhancing peroxidase-like activity of catalyst. The binding energies of C 1s and N1s signals for g-C_3N_4 and 10% Zn-mpg-C_3N_4 samples was very close to each other, but integral intensity of these signals was decreased with Zn doping. Compared to g-C_3N_4, the percentage of C-NH_2/C-NH in 10% Zn-mpg-C_3N_4 was decreased. This decrease in percentage indicated that thin nanosheets of 10% Zn-mpg-C_3N_4 was formed during the heat treatment of mixture of melamine, PEG-1500 and $ZnCl_2$•$2H_2O$. From these observations, we can conclude that aromatic units of g-C_3N_4 was somewhat broken by the Zn doping. Based on XPS and XRD analysis, we believed that the product obtained from the calcination of melamine, PEG-1500 and $ZnCl_2$•$2H_2O$ are basically Zn-doped mpg-C_3N_4.

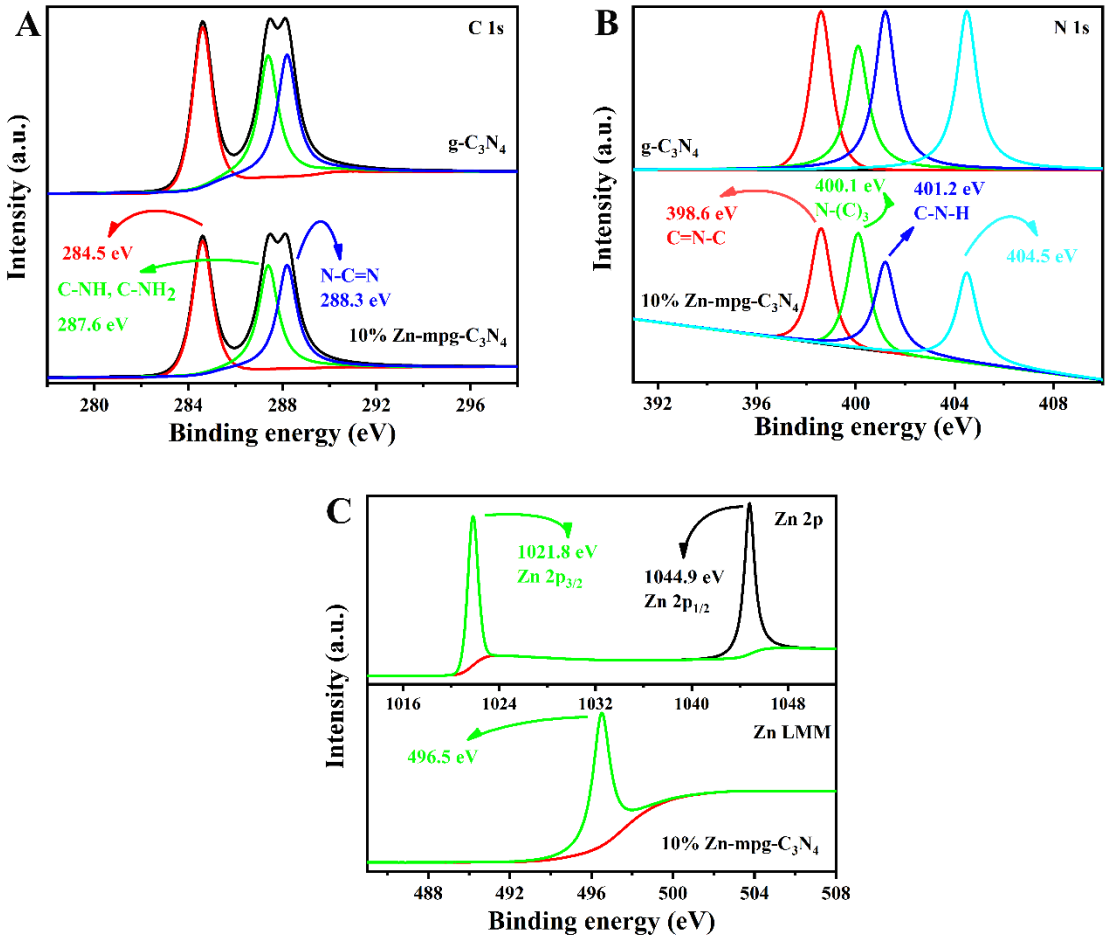

Figure 5. XPS spectra of C1s (A), N1s (B), Zn 2p and Auger Zn LMM (C) peaks of the samples.

In FTIR spectra (Figure 6), all characteristics absorption peaks in mpg-C_3N_4 and Zn doped mpg-C_3N_4 were almost like to that as in the case of g-C_3N_4. This showed that graphitic network in Zn doped mpg-C_3N_4 were similar with the network of g-C_3N_4. This revealed that Zn loading and use of PEG-1500 were not able to modify or change the basic structure and central chemical skeleton in modified g-C_3N_4 samples. Typical bands around 800 cm^{-1} in finger print region was assigned to breathing vibration of tri-s-triazine / s-triazine ring sextant out of the plan bending system, which was linked by -NH- group. High intensity broad absorbance bands in the range of 1225 - 1572 cm^{-1} was assigned to aromatic heterocyclic stretching vibration in C=N and C-NH-C

in finger print region likely derivative of s-triazine. Small absorption peaks around 2300 - 2404 cm^{-1} was assigned to -C≡N terminal groups and to the cumulated bonds (-N=C=N-) or alike species. A low intensity and broad set of peaks were found above 3000 cm^{-1}, which were attributed to the vibrational stretching mode in primary ($-NH_2$) or secondary (-NH) amine. These bands clearly indicated the presence of dandling hydrogen atoms in -C-N layers in all synthesized nanomaterials.

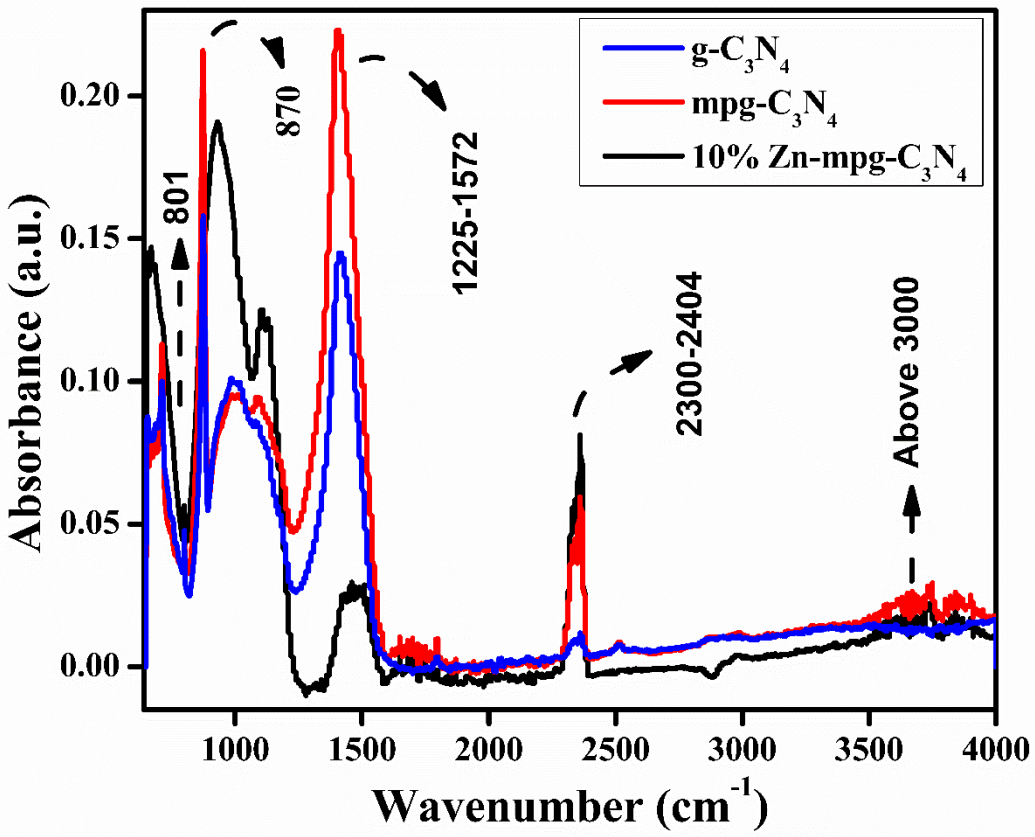

Figure 6. FTIR spectra of g-C_3N_4 based modified samples.

UV-Vis DRS analysis of pure g-C_3N_4 and Zn modified mpg-C_3N_4 were done by comparing spectra. As shown in Figure 7, Zn doped mpg-C_3N_4 spectrum exhibited strong absorption in the whole visible region. Absorption below 450 nm to the near-ultraviolet was resulted from the charge transfer response of g-C_3N_4 and its functionalized materials from valence-band occupied by N 2p

orbitals to conduction-band resulted from C 2p orbitals. Absorption peaks in UV region was attributed to the band gap of polymeric melon units of g-C_3N_4. Absorption edge of Zn doped mpg-C_3N_4 showed a shift in wavelength region as the dopant concentration was varied. It was decreased, reached its minimum value and then increased with respect to the dopant concentration. Estimated band gap was calculated using formula (Band gap = 1240 / Absorption edge (λ)) in electron volt (eV). Insert in Figure 7 showed that g-C_3N_4 has band gap of 2.74 eV, whereas Zn doped mpg-C_3N_4 possessed band gap of 2.94, 2.95, 2.96, 2.99, 2.99, 3.0, 2.98, 2.96 and 2.93 eV for different wt. percentage of Zn content as 0, 1, 2.2, 3.3, 4.7, 10, 15, 38 and 52 in mpg-C_3N_4 respectively. This variation in band gap with Zn dopant was originated due to the repulsive interaction of 3d orbitals of host (Zn) and 2p orbitals of guest (nitrogen) in doped g-C_3N_4.[33] It can also be seen that Zn doped mpg-C_3N_4 has higher absorbance intensity in UV region, whereas less absorbance in visible region than g-C_3N_4. These variations in spectra indicated that Zn was coordinated with π-conjugated system of g-C_3N_4, and doping strategy was useful for tuning the band gap and to facilitate the charge transfer in aromatic CN heterocyclic conjugated system.[33]

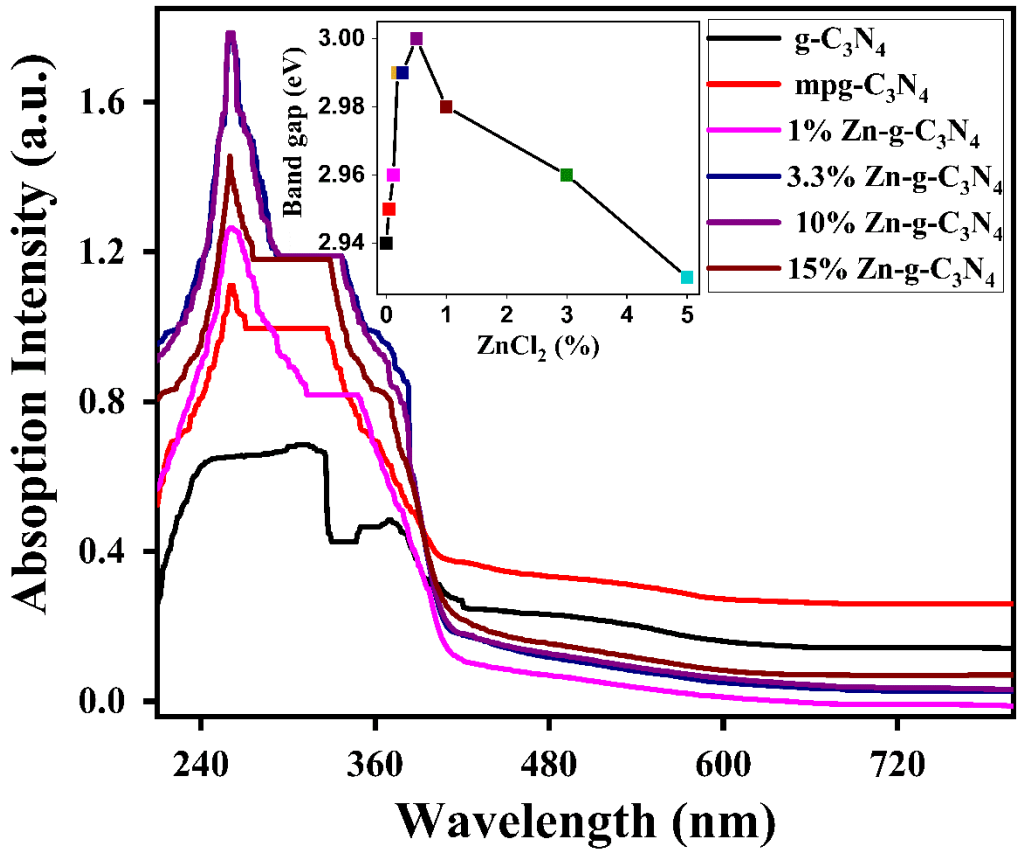

Figure 7. UV-Visible DRS spectra (insert showed the change in band gap with respect to dopant amount) of g-C_3N_4 and its modified forms.

Raman spectra (Figure S2) showed the coordination of Zn species and maintenance of graphitic structure in the synthesized samples.[34] PL spectra (Figure 8) under an excitation wavelength of 457 nm was scanned and observed a main PL emission around 588 nm in the spectra of all the samples. The PL intensity of g-C_3N_4 sample was more than the PL intensity of mpg-C_3N_4. PL intensity was depended on the dopant concentration and was quenched with the increase in Zn loading, reached to minimum value, after that it was began to increase. It can be seen in Figure 8 that PL intensity of 10% Zn-mpg-C_3N_4 was lowest due to loading of optimum Zn content. At optimum Zn loading, recombination of photo generated charge carriers was inhibited and an

enhancement in electron-hole transfer between Zn and mpg-C_3N_4 was occurred. This factor increased the availability of more holes for oxidation of TMB. Therefore, metallic elemental doping strategy was useful to tune the electronic related properties, photo generated charge carrier's recombination and electronic transferability in the samples.[35]

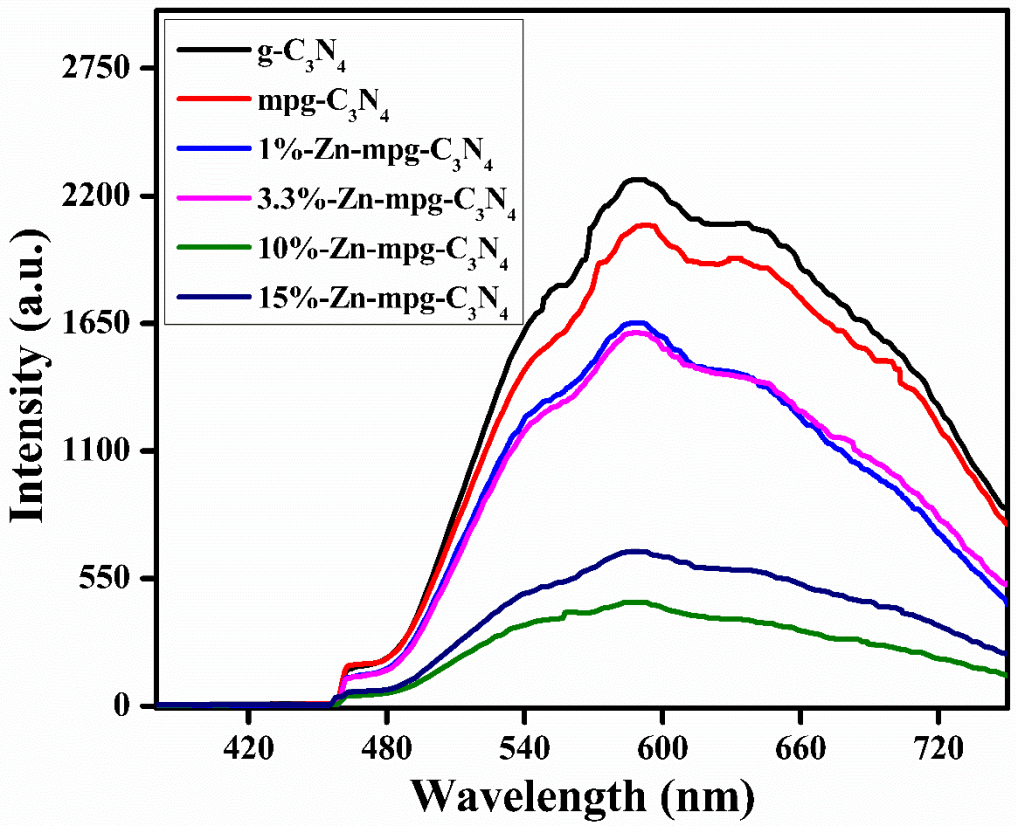

Figure 8. PL spectra at excitation wavelength of 457 nm of g-C_3N_4 and Zn modified mpg-C_3N_4.

3.1 Peroxidase-Activity of Nanosheets

A comparison of peroxidase-like activity of g-C_3N_4, mpg-C_3N_4 and 10% Zn-mpg-C_3N_4 is shown in term of their UV-Vis absorption spectra in Figure 9A.

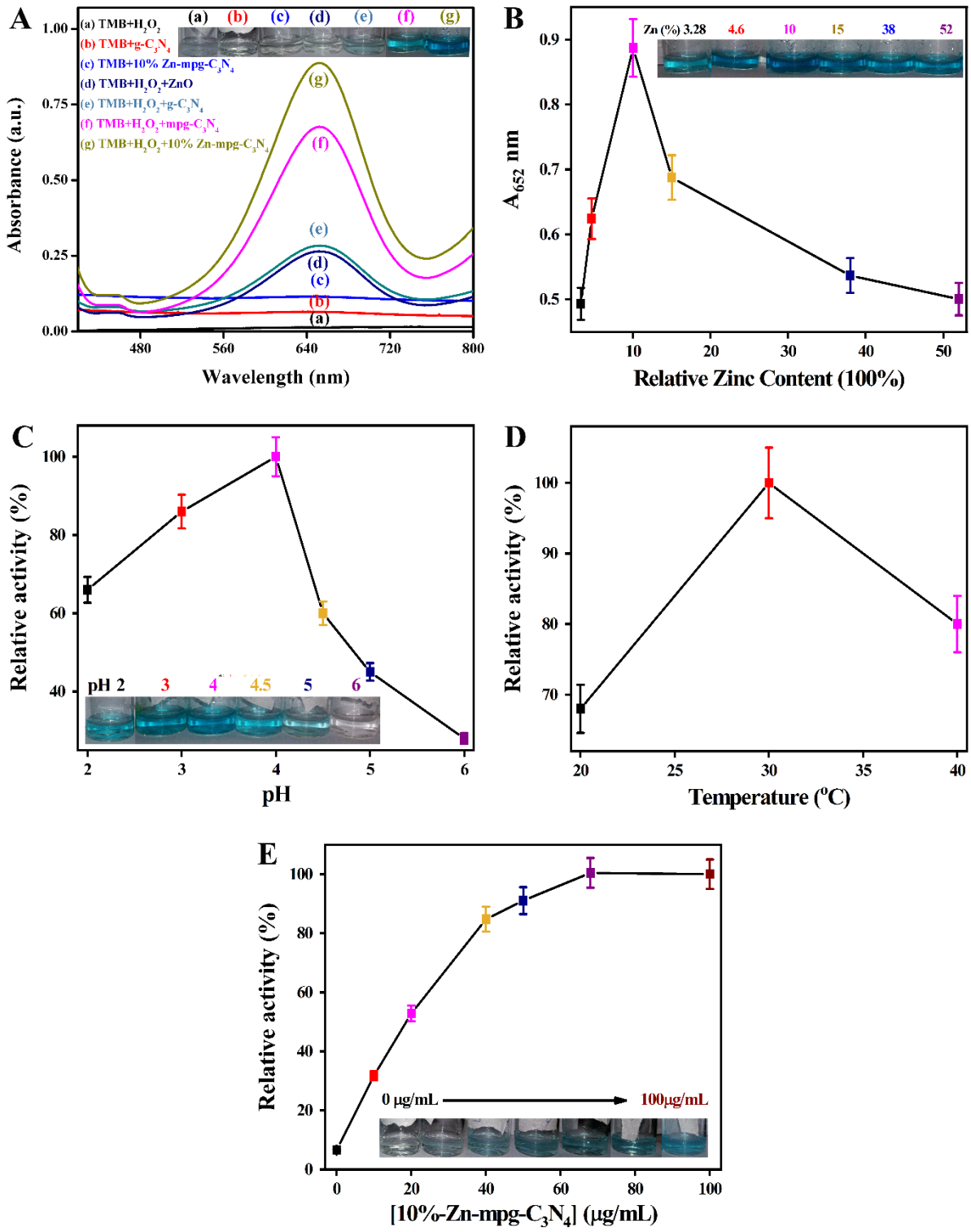

Figure 9. UV-Vis absorption spectra for comparison of peroxidase-like activity after one-hour incubation of the reaction mixture (A) Effect of dopant concentration (B) pH (C) temperature (D)

and catalyst concentration (E) on peroxidase-like activity. The reaction mixture containing 68 µg mL^{-1} nanosheets, 300 µM TMB, 400 µM of H_2O_2 in sodium acetate buffer (pH 4.0, 100 mM). Inserts showed the digital images of color change in the reaction systems.

The A_{652} nm was linked to the charge-transfer complexes resulting from one-electron oxidation of TMB and reaction mixtures were turned to a blue color (Insert of Figure 9A). It is clear from Figure 9A, that A_{652} nm of 10% Zn-mpg-C_3N_4 (curve g) reaction mixture was higher than that of A_{652} nm of mpg-C_3N_4 (curve f), g-C_3N_4 (curve e), and ZnO (curve d) reaction systems. This indicated that Zn ions coordination in thin mesoporous nanosheets of g-C_3N_4 has displayed a major role for enhancing peroxidase-like catalytic activity. In turn, many light-triggered reactive oxygen species were generated due to the presence of more catalytic active sites and novel functionalities in Zn-mpg-C_3N_4. Effect of precursor PEG-1500 in the synthesis of mpg-C_3N_4 can be clearly observed, when a comparison of A_{652} nm of mpg-C_3N_4 (curve f) was done with the A_{652} nm of the simple g-C_3N_4 (curve e) and ZnO (curve d). The A_{652} nm of mpg-C_3N_4 reaction system was higher than the A_{652} nm of g-C_3N_4 and ZnO reaction systems. This higher peroxidase-like catalytic activity of mpg-C_3N_4 was attributed to its thin and porous morphology as compared to simple g-C_3N_4 and ZnO. Further, in the absence of H_2O_2 the reaction system consisting of g-C_3N_4 nanosheets and TMB has displayed no obvious change (curve b), which indicated that no redox reaction occurred. In contrast, in the absence of H_2O_2 the reaction between 10% Zn-mpg-C_3N_4 nanosheets and TMB has displayed small change in color (curve c). These observations indicated the higher electron transferability, higher charge separation efficiency and higher intrinsic peroxidase-like activity of 10% Zn-mpg-C_3N_4 nanosheets as compared to that of the pure g-C_3N_4 nanosheets. Therefore, Zn doping has enabled electron coupling between Zn metals and mpg-C_3N_4 by shaped unique electronic structures. These unique electronic structures favored the electron

mobilization along the electronically delocalized planar thin nanosheets by accelerating the electron transfer process. There was no peak at A_{652} nm and no blue color in the reaction mixture was observed, when TMB was mixed with H_2O_2 (curve a) in the absence of nanosheets. These observations indicated that the reaction may be occurred only, if catalyst nanosheets were present in the reaction mixture.

3.2 Optimization of Reaction Conditions

Catalytic action for H_2O_2 detection was mainly depended on the reaction conditions, which were included as pH, temperature, concentration of dopant, amount of nanosheets, [TMB] etc. Therefore, optimization of these conditions was paramount important. The amount of Zn content was varied from 0 to 52% with respect to mpg-C_3N_4 and the effect of this variation in ratio of Zn to mpg-C_3N_4 on peroxidase-like activity of the catalyst was investigated. It was observed that the peroxidase-like activity of nanosheets was dramatically decreased at high nanosheets concentration. Therefore, Zn to mpg-C_3N_4 ratio was needed to be optimized with respect to Zn concentration. The effect of various dopant percentages in mpg-C_3N_4 on A_{652} nm was shown in Figure 9B. The A_{654} nm was decreased, when the relative Zn doping content was exceeds from 10%. This effect was attributed to the decrease in electron transferability, production of excessive lattice defects and generation of recombination sites for the charge carriers. It was clear from Figure 9B that among doped samples, only 10% Zn-mpg-C_3N_4 possessed higher peroxide like activity. So, the optimum relative Zn content value in the sample was determined as 10%, which was corresponding to mass ratio of 1:0.1 between Zn and mpg-C_3N_4. Kinetics study of the reaction system was performed by measuring A_{652} nm with respect to time. A comparison of kinetics curves of TMB-H_2O_2 for g-C_3N_4 and 10% Zn-mpg-C_3N_4 under the same reaction conditions showed that reaction rate of Zn doped catalyst was better than that of g-C_3N_4. This revealed that peroxidase-

like activity as well as kinetics of the reaction was improved by Zn modification in the catalyst. This improvement was related to the presence of Zn-N active sites in the porous morphology, high electron transferability, and low recombination rate due to capturing of conduction band electrons by Zn ions and enlargement in surface area to provide greater catalytic active sites for 10% Zn-mpg-C_3N_4 as compared to pure g-C_3N_4.

The pH of acetate buffer was optimized in range from 2.0 - 6.0 and temperature was optimized in the range from 20 - 40°C. Effect of change in pH and change in temperature on 10% Zn-mpg-C_3N_4 catalytic activity was presented in Figure 9C and Figure 9D respectively. Optimal pH for the system was calculated as 4.0, which showed that stable catalytic activity of nanosheets and TMB oxidation befall in weak acidic condition as already been reported for some other nanomaterials.[6, 24, 33, 36-37] Furthermore, the relative activity of reaction system was better at 30°C, which indicated that our material worked well near room temperature. The effect of amount of 10% Zn-mpg-C_3N_4 nanosheets on peroxidase-like activity was determined by investigating time dependent absorbance change against various amount of 10% Zn-mpg-C_3N_4 from 0 - 100 µg mL^{-1}. It can be seen form Figure S3 that A_{652} nm was increased as the concentration of nanosheets suspension was increased and time was prolonged. The maximum reaction level was observed at 68 µg mL^{-1}. A linear relationship between sample amount and catalytic activity was obtained as depicted in Figure 9E. However, it can be seen in figure that at higher nanosheets concentration deviation from linearity was occurred.

3.3 Mechanism and Steady-State Catalytic Kinetics Assay of H_2O_2 Using 10% Zn-mpg-C_3N_4 Nanosheets

To explore mechanism of peroxidase-like catalytic activity of 10% Zn-mpg-C_3N_4, steady-state kinetics assay was performed by keeping concentration of substrate constant, while varying

concentration of analyte. Kinetics curves are shown in Figure S4, when [TMB] (300 µM) was kept fixed and [H_2O_2] was varied. Similar kinetics curves in Figure S5 are obtained, when [H_2O_2] (400 µM) was fixed and [TMB] was varied. As excessive [H_2O_2] or [TMB] inhibited the rate of reaction, so equilibrium concentrations were required to be determined.

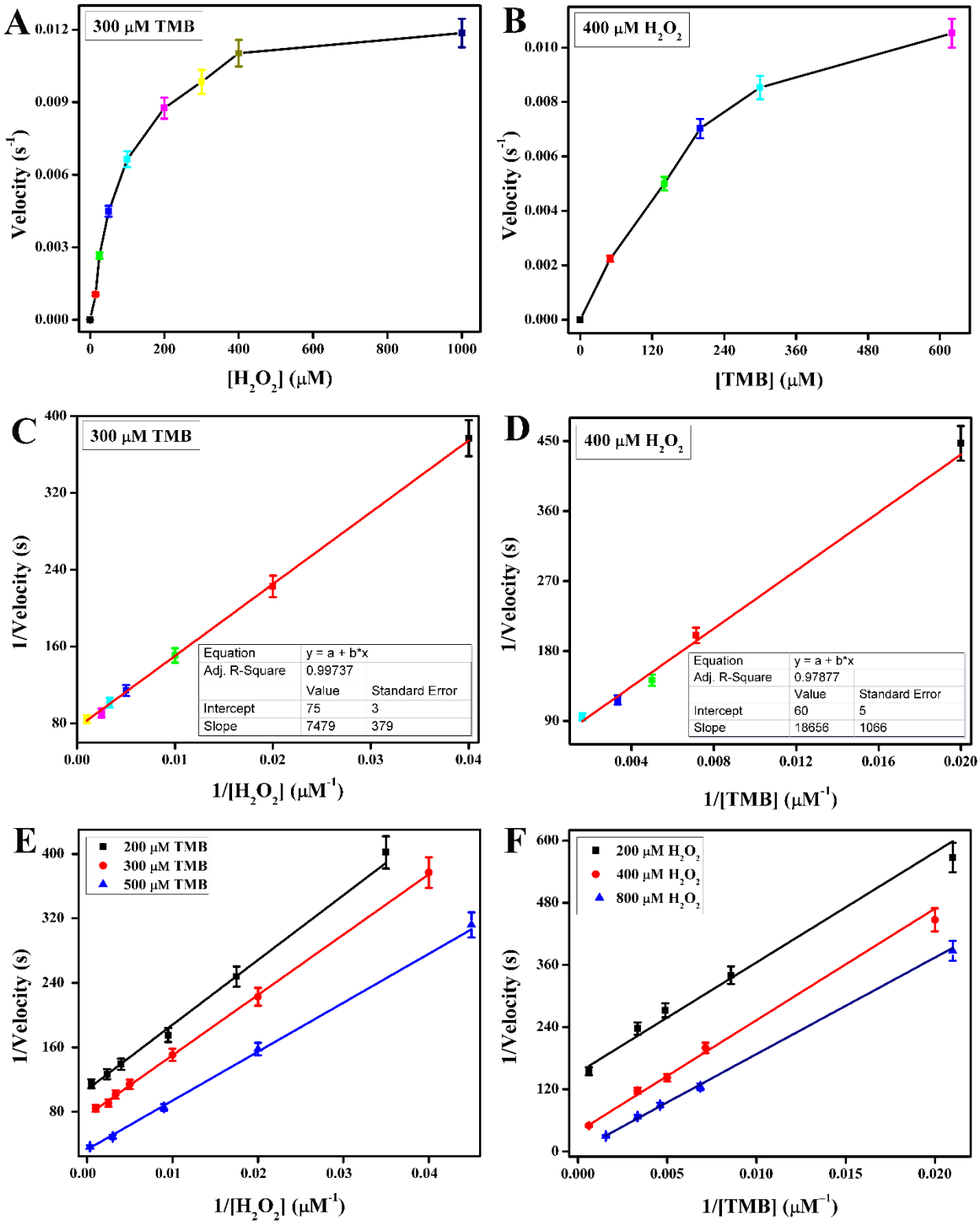
A
300 μM TMB
Velocity (s^{-1})
[H_2O_2] (μM)
B
400 μM H_2O_2
Velocity (s^{-1})
[TMB] (μM)
C
300 μM TMB
1/Velocity (s)
1/[H_2O_2] (μM^{-1})
Equation y = a + b*x
Adj. R-Square 0.99737
Value Standard Error
Intercept 75 3
Slope 7479 379
D
400 μM H_2O_2
1/Velocity (s)
1/[TMB] (μM^{-1})
Equation y = a + b*x
Adj. R-Square 0.97877
Value Standard Error
Intercept 60 5
Slope 18656 1066
E
200 μM TMB
300 μM TMB
500 μM TMB
1/Velocity (s)
1/[H_2O_2] (μM^{-1})
F
200 μM H_2O_2
400 μM H_2O_2
800 μM H_2O_2
1/Velocity (s)
1/[TMB] (μM^{-1})

Figure 10. Michaelis-Menten curves of 10% Zn-mpg-C_3N_4 for H_2O_2 (A) and for TMB (B). Double reciprocal plot for H_2O_2 (C) and for TMB (D). Ping-Pong mechanism for H_2O_2 (E) and TMB (F).

Apparent steady-state reaction rates and initial velocity for both TMB and H_2O_2 were determined by calculating the slopes of linear portion of absorbance changes at 652 nm with time curves. The concentration of oxidized TMB ($TMB^{\bullet+}$) was determined by applying the Beer-Lambert law ($A = \varepsilon Cl$, where A was absorbance, 'l' was path length (l = 1 cm), C is concentration of substrate and ε was extinction coefficient (ε = 39,000 M^{-1} cm^{-1}) respectively). Typical Michaelis-Menten curves were drawn for suitable range of H_2O_2 and TMB as shown in Figure 10A and Figure 10B respectively. The value of K_m affects the reaction kinetics and represents the binding affinities of catalytic nanomaterials to the substrate. Table 2 represents the relationship between K_m, nanomaterials and substrates. The smaller K_m represents the stronger affinity in catalytic nanomaterials and substrates.

Table 2. Comparison of K_m and V_{max} of horseradish peroxide (HRP), g-C_3N_4, mpg-C_3N_4 and 10% Zn-mpg-C_3N_4.

Catalyst	**Substrate**	**K_m (mM)**	**V_{max}**	**Ref.**
10% Zn-mpg-C_3N_4	TMB	0.1	1.33 (10^{-8} Ms^{-1})	Present work
	H_2O_2	0.311	1.7 (10^{-8} Ms^{-1})	
HRP	TMB	0.275	1.24 (10^{-8} Ms^{-1})	[38]
	H_2O_2	0.214	2.46 (10^{-8} Ms^{-1})	
Co-g-C_3N_4-2	TMB	0.113	8.46 (10^{-8} Ms^{-1})	[33]
	H_2O_2	318.58	9.46 (10^{-8} Ms^{-1})	
MnSe-g-C_3N_4	TMB	0.137	2.40 (10^{-3} s^{-1})	[37]
	H_2O_2	0.623	2.85 (10^{-3} s^{-1})	
Cu NPs/g-C_3N_4	TMB	0.389	5.84 (10^{-7} s^{-1})	[36]
	H_2O_2	9.27	3.84 (10^{-7} s^{-1})	

g-C_3N_4	TMB	0.031	1.35 (10^4 Ms^{-1})	3
	H_2O_2	4.565	1.72 (10^4 Ms^{-1})	
Fe-g-C_3N_4	TMB	0.030	1.95 (10^4 Ms^{-1})	3
	H_2O_2	8.956	1.46 (10^4 Ms^{-1})	
Se-g-C_3N_4	TMB	0.307	20.5 (10^{-4} s^{-1})	24
	H_2O_2	0.298	43.3 (10^{-4} s^{-1})	

Apparent K_m value of 10% Zn-mpg-C_3N_4 nanosheets with TMB substrate (0.1 mM) was three times lower than K_m of HRP (0.275 mM) with TMB substrate. This was attributed to high surface area of several small pores on nanosheets and presence of more catalytic active sites on the porous material, which resulted in strong adsorption affinity between carbon nitride nanosheets and TMB as compared to the natural HRP. The reaction rate at saturation point of nanozymes with substrate was explained by V_{max} values. The V_{max} of 10% Zn-mpg-C_3N_4 with TMB substrate (1.33×10^{-8} Ms^{-1}) was 1.1 times higher than that of natural HRP (1.24×10^{-8} Ms^{-1}), which represented a higher reaction rate of 10% Zn-mpg-C_3N_4 nanosheets. This was attributed to intrinsic electron transfer capability of graphitic-structure and presence of Zn content in the nanosheets. The catalytic activity of nanosheets was highly efficient and was like natural enzymes. The K_m value of 10% Zn-mpg-C_3N_4 for H_2O_2 substrate (0.311 mM) was 1.5 times higher than K_m value (0.214 mM) of natural HRP, which was consistent with the observation that a higher [H_2O_2] was required to achieve maximal activity for 10% Zn-mpg-C_3N_4 nanosheets. Double-reciprocal plots between initial velocities against various [H_2O_2] analyte by keeping substrate [TMB] constant and vice versa are shown in Figure 10C and Figure 10D respectively. Graphs showed that the reaction catalyzed by 10% Zn-mpg-C_3N_4 nanosheets followed typical Michaelis-Menten model. A comparison of double-reciprocal plots between initial velocities with variable [H_2O_2] against three

[TMB] (200, 300 and 500 μM) substrates and variable [TMB] against three [H_2O_2] (200, 400 and 800 μM) substrates were carried out to investigate Ping-Pong mechanism as depicted in Figure 10E and 10F respectively. Double reciprocal plots were characterized by straight parallel lines and showed a Ping-Pong mechanism for these nanomaterials as shown by HRP. Ping-Pong mechanism is a mechanism of a non-sequential double-displacement enzymatic reaction in which enzyme is changed to an intermediate form, when first reacting substrate is changed to the product. This intermediate form of enzyme is temporary and changes to standard form by bouncing back and forth to change the second reacting substrate to product. In this mechanism, enzyme is acted like a Ping-Pong ball. In steady-state catalytic kinetics assay, a reaction follow Ping-Pong mechanism, when a plot between 1 / Velocity against 1 / [First substrate] at varying concentrations of second substrate is a series of parallel lines and vice versa as shown in Figure 10E and 10F. It means that Zn-mpg-C_3N_4 nanosheets responded to first reacting substrate to release product of this substrate before responding with second reacting substrate. Such, catalytic mechanism of reaction was associated with the π–conjugated electronic structures of 10% Zn-mpg-C_3N_4 nanosheets and its affinities with substrates like H_2O_2 and TMB. Catalyst nanosheets were π–rich and could adsorbed TMB via π–π interaction. Due to proximity, electron transfer was occurred from lone pair of amino groups of TMB to catalyst nanosheets, which resulted in the oxidation of TMB. Electrons would transfer from nanosheets to H_2O_2. Product from this substrate was hydroxyl radicals due to the decomposition of H_2O_2 under the catalytic effect of 10% Zn-mpg-C_3N_4 nanosheets. Hydroxyl radicals facilitated the oxidation of TMB. Possible reaction mechanism of peroxidase-like catalytic activity of 10% Zn-mpg-C_3N_4 nanosheets was shown in Scheme 1. Similarly, other metal coordinated (Cu^{2+}, Pd NPs, Co^{3+}, MnSe NPs, Fe^{3+}) peroxidase-mimic catalyst of g-C_3N_4 has been reported. From rest of these, our synthesized Zn^{2+} coordinated thin mesoporous nanosheets of g-

C_3N_4 has displayed better kinetics and catalytic activity. This indicated that our prepared nanomaterial has more catalytic active sites and has generated many light-triggered reactive oxygen species due to presence of novel functionalities in it.

3.4 Sensing of H_2O_2

Graphitic structure facilitates the electron transfer process and such structure type aromatic carbon compounds exhibit intrinsic peroxidase-like activity. The reduction of H_2O_2 takes place via an electron transfer process by donation of electrons from carbon network on micro level. This electron transfer process can be enhanced through different techniques such as metallic doping and nano-structuring. Therefore, for better peroxidase-like activity of nanosheets, it was supposed that Zn doped mpg-C_3N_4 would serve as natural enzyme and may be used as catalyst in H_2O_2 reduction. Nanosheets activity was determined by the amount of oxidized TMB in H_2O_2 by UV-Vis absorption spectra. It was noted that oxidized TMB imparted blue color to the reaction mixture, which was corresponding to a maximum absorption intensity at 652 nm. Without nanosheets, the reaction mixture containing H_2O_2, TMB or both in sodium acetate buffer gave no blue color, so no oxidation of TMB occurred. However, upon the addition of nanosheets in reaction system, oxidation of TMB was occurred and a blue color was developed with an absorption maxima at 652 nm. This was the indication of nanosheets catalytic activity.

According to excellent peroxidase-like activity of our synthesized 10% Zn-mpg-C_3N_4 nanosheets under optimum experimental conditions of pH, temperature, [TMB] and nanosheets amount, a colorimetric sensor for the detection of H_2O_2 using TMB substrate was developed. Using typical [H_2O_2] and sensor response, UV-Vis absorption curves under optimum experimental conditions (pH 4.0, 25^{o}C) were obtained and shown in Figure 11A.

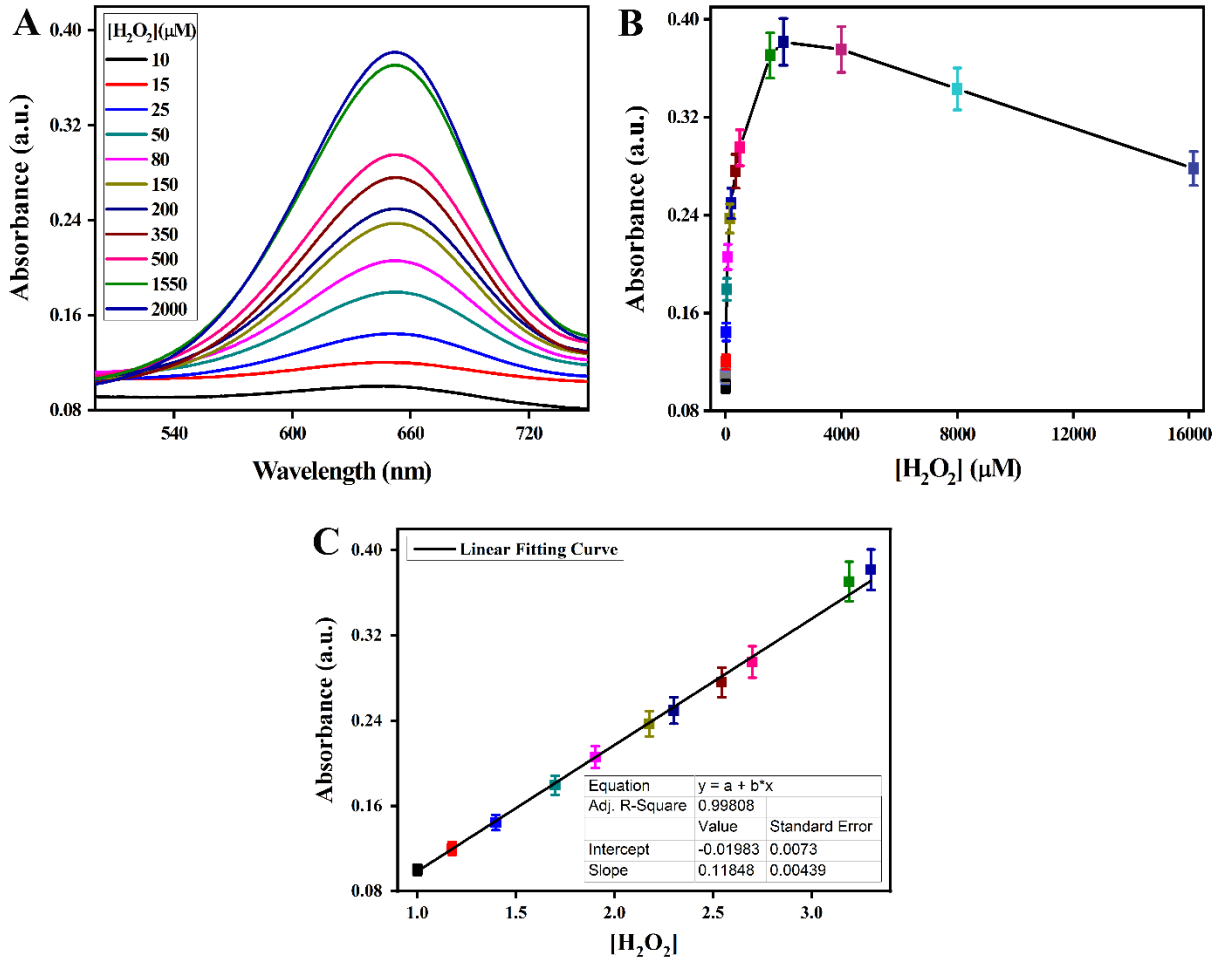

Figure 11. Typical UV-Visible absorption spectra (A), sensor dose response curve (B), and linear-calibration plot (C).

Graph between absorbance at lambda max (λ_{max}) of 652 nm versus [H_2O_2] in the presence of nanosheets is shown in Figure 11B. Absorption intensity was increased as [H_2O_2] was varied between 0 - 2000 µM, while at higher [H_2O_2] peroxidase-like activity of catalyst was inhibited. There was a slight increase in absorption intensity beyond 400 µM of [H_2O_2], which was supposed as reaction equilibrium [H_2O_2]. A linear range of the sensor was determined from linear calibration curve as 10 - 2000 µM using absorbance versus [H_2O_2] as depicted in Figure 11C. Quantification limit (LOQ) and detection limit (LOD) of developed H_2O_2 sensor were found from linear

regression-equation of H_2O_2 dose and response curve by using 10σ/s and 3.3σ/s respectively. Sigma (σ) and (s) are standard error of estimate and slop of linear regression-line respectively. LOD was obtained as low as 1.4 μM and LOQ as 3.0 μM. Table 3 represented a comparison of linear ranges and LODs of different g-C_3N_4 based colorimetric sensors.

Table 3. Comparison of linear ranges, LODs of different nanomaterials as peroxidase mimetic for H_2O_2 assays.

Materials	**Linear Range (μM)**	**LOD (μM)**	**Reference**
10% Zn-mpg-C_3N_4	10 - 2000 (R^2 = 0.9981)	1.4	Present Work
g-C_3N_4	1 - 100 (R^2 = 0.994)	0.4	[39]
Utg-C_3N_4 NSs	10 - 100 (R^2 = 0.9902)	5.6	[40]
g-C_3N_4	5 - 30 (R^2 = 0.9866)	0.9	[2]
Se-g-C_3N_4	16 – 4000	1.6	[24]
MeSe-g-C_3N_4	18 - 1800 (R^2 = 0.9986)	1.8	[37]

4. CONCLUSION

In summary, we have used calcination method to synthesize g-C_3N_4 and thin porous Zn doped mpg-C_3N_4 by using mixture of melamine, PEG-1500 and zinc chloride. Introduction of PEG-1500 as soft template in reaction mixture was beneficial for the enhancement in porosity and to increase in amount of Zn loading in the graphitic framework of g-C_3N_4. Results indicated that Zn-mpg-C_3N_4 possessed enhanced intrinsic peroxidase-like activity. The synergistic effects of high conductivity, electron transfer capability of mpg-C_3N_4 support and intrinsic peroxidase-like activity of Zn doping, facilitated in enhancement of peroxidase-like catalysis. Steady-state kinetics analysis specified that catalysis followed Ping-Pong mechanism. In the presence of 10% Zn-mpg-C_3N_4 nanosheets, TMB and H_2O_2 were reacted and reaction mixture color was turned to blue,

which was the basis for the development of a colorimetric assay for H_2O_2. Peroxidase-mimics activity of 10% Zn-mpg-C_3N_4 has presented several advantages over natural enzymes such as facile preparation, low cost, fast response and high stability, which might be allowed this nanomaterial to be used as an enzyme free peroxidase-mimics for potential applications in biotechnology and medical diagnostic areas.

ASSOCIATED CONTENT

Supporting Information

The supporting information (PDF) includes Figure S1 to S5 for EDX images and analysis, Raman spectra, kinetics study of different amount of catalyst, steady state kinetics assay at fix [TMB] and variable [H_2O_2] and vice versa. The supporting information is available free of charges on the ACS Publications website at http://pubs.acs.org.

AUTHOR INFORMATION

Corresponding author

*Muhammad Nasir: muhammadnasir@cuilahore.edu.pk

*Akhtar Hayat: akhtarhayat@cuilahore.edu.pk

ORCID iD

Muhammad Nasir: 0000-0002-6742-2721

Author Contributions

All authors have contributed and approved the final version of the manuscript.

Funding Sources

This work was supported by Higher Education Commission Pakistan through its NRPU grant 20-4993/R&D/HEC/14 and Pakistan Science Foundation and National Natural Science Foundation China through its PSF-NSFC funded project (Project No. PSF/NSFC-II/Eng/P-COMSATS-Lhr (07).

Notes

The authors declare no competing financial interest.

ACKNOWLEDGMENT

Aftab Ahmed thanks Interdisciplinary Research Centre in Biomedical Materials (IRCBM), COMSATS University Islamabad, Lahore Campus to allow him to use its facility for the execution of his research work and acknowledges the efforts his seniors and fellow colleagues in guiding him to complete it.

TOC Graphic

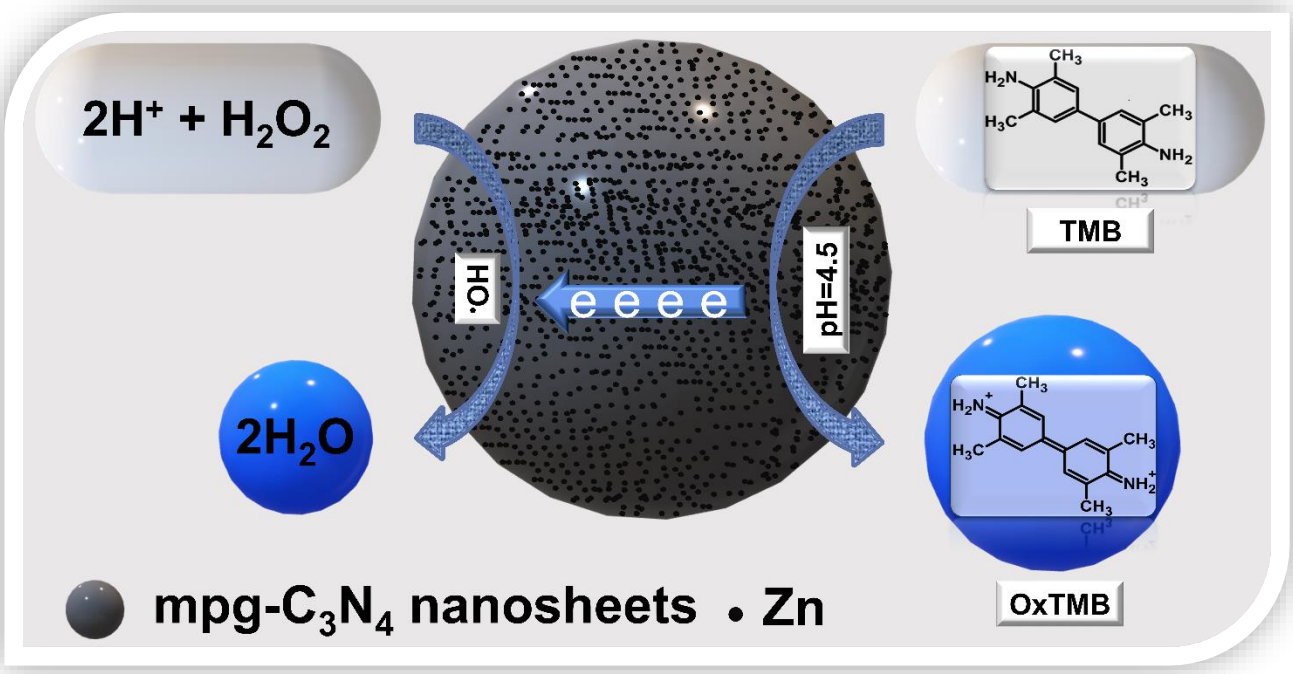

REFERENCES

(1) Salimi, A.; Hallaj, R.; Soltanian, S.; Mamkhezri, H. Nanomolar detection of hydrogen peroxide on glassy carbon electrode modified with electrodeposited cobalt oxide nanoparticles. *Anal Chim Acta* **2007**, 594, 24-31.

(2) Lin, T.; Zhong, L.; Wang, J.; Guo, L.; Wu, H.; Guo, Q.; Fu, F.; Chen, G. Graphite-like carbon nitrides as peroxidase mimetics and their applications to glucose detection. *Biosensors and Bioelectronics* **2014**, 59, 89-93.

(3) Tian, J.; Liu, Q.; Asiri, A. M.; Qusti, A. H.; Al-Youbi, A. O.; Sun, X. Ultrathin graphitic carbon nitride nanosheets: a novel peroxidase mimetic, Fe doping-mediated catalytic performance enhancement and application to rapid, highly sensitive optical detection of glucose. *Nanoscale* **2013**, 5, 11604-9.

(4) Tian, H.; Fan, H.; Ma, J.; Ma, L.; Dong, G. Noble metal-free modified electrode of exfoliated graphitic carbon nitride/ZnO nanosheets for highly efficient hydrogen peroxide sensing. *Electrochimica Acta* **2017**, 247, 787-794.

(5) Xi, X.; Li, J.; Wang, H.; Zhao, Q.; Li, H. Non-enzymatic photoelectrochemical sensing of hydrogen peroxide using hierarchically structured zinc oxide hybridized with graphite-like carbon nitride. *Microchimica Acta* **2015**, 182, 1273-1279.

(6) Vazquez-Gonzalez, M.; Liao, W. C.; Cazelles, R.; Wang, S.; Yu, X.; Gutkin, V.; Willner, I. Mimicking Horseradish Peroxidase Functions Using Cu(2+)-Modified Carbon Nitride Nanoparticles or Cu(2+)-Modified Carbon Dots as Heterogeneous Catalysts. *ACS Nano* **2017**, 11, 3247-3253.

(7) Breslow, R. Biomimetic Chemistry and Artificial Enzymes: Catalysis by Design. *Accounts of Chemical Research* **2002**, 28, 146-153.

(8) Hu, P.; Han, L.; Zhu, C.; Dong, S. J. Nanoreactors: a novel biosensing platform for protein assay. *Chemical Communications* **2013**, 49, 1705-1707.

(9) Wu, J.; Wang, X.; Wang, Q.; Lou, Z.; Li, S.; Zhu, Y.; Qin, L.; Wei, H. Nanomaterials with enzyme-like characteristics (nanozymes): next-generation artificial enzymes (II). *Chem Soc Rev* **2019**, 48, 1004-1076.

(10) Wei, H.; Wang, E. Nanomaterials with enzyme-like characteristics (nanozymes): next-generation artificial enzymes. *Chem Soc Rev* **2013**, 42, 6060-93.

(11) Lin, Y.; Ren, J.; Qu, X. Catalytically active nanomaterials: a promising candidate for artificial enzymes. *Acc Chem Res* **2014**, 47, 1097-105.

(12) He, L.; Su, Y.; Lanhong, J.; Shi, S. Recent advances of cerium oxide nanoparticles in synthesis, luminescence and biomedical studies: a review. *Journal of Rare Earths* **2015**, 33, 791-799.

(13) Challier, L.; Gal, F.; Carrot, G.; Perez, H.; Noel, V. Hybrid platinum nanoparticle ensemble for the electrocatalytic oxidation of H2O2: Toward nanostructured biosensor design. *Electrochemistry Communications* **2013**, 28, 118-121.

(14) Nasir, M.; Rauf, S.; Muhammad, N.; Hasnain Nawaz, M.; Anwar Chaudhry, A.; Hamza Malik, M.; Ahmad Shahid, S.; Hayat, A. Biomimetic nitrogen doped titania nanoparticles as a colorimetric platform for hydrogen peroxide detection. *J Colloid Interface Sci* **2017**, 505, 1147-1157.

(15) Gao, L.; Zhuang, J.; Nie, L.; Zhang, J.; Zhang, Y.; Gu, N.; Wang, T.; Feng, J.; Yang, D.; Perrett, S.; Yan, X. Intrinsic peroxidase-like activity of ferromagnetic nanoparticles. *Nat Nanotechnol* **2007**, 2, 577-83.

(16) Cheng, X.; Huang, L.; Yang, X.; Elzatahry, A. A.; Alghamdi, A.; Deng, Y. Rational design of a stable peroxidase mimic for colorimetric detection of H2O2 and glucose: A synergistic CeO2/Zeolite Y nanocomposite. *Journal of Colloid and Interface Science* **2019**, 535, 425-435.

(17) Ge, J.; Yang, X.; Luo, J.; Ma, J.; Zou, Y.; Li, J.; Luo, W.; Cheng, X.; Deng, Y. Ordered mesoporous CoO/CeO2 heterostructures with highly crystallized walls and enhanced peroxidase-like bioactivity. *Applied Materials Today* **2019**, 15, 482-493.

(18) Wang, H.; Wan, K.; Shi, X. Recent Advances in Nanozyme Research. *Adv Mater* **2018**, e1805368.

(19) Zhou, Y.; Liu, B.; Yang, R.; Liu, J. Filling in the Gaps between Nanozymes and Enzymes: Challenges and Opportunities. *Bioconjug Chem* **2017**, 28, 2903-2909.

(20) Wang, X.; Maeda, K.; Thomas, A.; Takanabe, K.; Xin, G.; Carlsson, J. M.; Domen, K.; Antonietti, M. A metal-free polymeric photocatalyst for hydrogen production from water under visible light. *Nat Mater* **2009**, 8, 76-80.

(21) Zhang, J.; Zhang, G.; Chen, X.; Lin, S.; Mohlmann, L.; Dolega, G.; Lipner, G.; Antonietti, M.; Blechert, S.; Wang, X. Co-monomer control of carbon nitride semiconductors to optimize hydrogen evolution with visible light. *Angew Chem Int Ed Engl* **2012**, 51, 3183-7.

(22) Li, X.; Zhu, L.; Zhou, Y.; Yin, H.; Ai, S. Enhanced Photoelectrochemical Method for Sensitive Detection of Protein Kinase A Activity Using TiO2/g-C3N4, PAMAM Dendrimer, and Alkaline Phosphatase. *Anal Chem* **2017**, 89, 2369-2376.

(23) Wang, H.; Qi, C.; He, W.; Wang, M.; Jiang, W.; Yin, H.; Ai, S. A sensitive photoelectrochemical immunoassay of N6-methyladenosine based on dual-signal amplification strategy: Ru doped in SiO2 nanosphere and carboxylated g-C3N4. *Biosensors and Bioelectronics* **2018**, 99, 281-288.

(24) Qiao, F.; Wang, J.; Ai, S.; Li, L. As a new peroxidase mimetics: The synthesis of selenium doped graphitic carbon nitride nanosheets and applications on colorimetric detection of H2O2 and xanthine. *Sensors and Actuators B: Chemical* **2015**, 216, 418-427.

(25) Wang, Y.; Wang, Y.; Li, Y.; Shi, H.; Xu, Y.; Qin, H.; Li, X.; Zuo, Y.; Kang, S.; Cui, L. Simple synthesis of Zr-doped graphitic carbon nitride towards enhanced photocatalytic performance under simulated solar light irradiation. *Catalysis Communications* **2015**, 72, 24-28.

(26) Xing, W.; Chen, G.; Li, C.; Sun, J.; Han, Z.; Zhou, Y.; Hu, Y.; Meng, Q. Construction of Large-Scale Ultrathin Graphitic Carbon Nitride Nanosheets by a Hydrogen-Bond-Assisted Strategy for Improved Photocatalytic Hydrogen Production and Ciprofloxacin Degradation Activity. *ChemCatChem* **2016**, 8, 2838-2845.

(27) Jiang, L.; Yuan, X.; Pan, Y.; Liang, J.; Zeng, G.; Wu, Z.; Wang, H. Doping of graphitic carbon nitride for photocatalysis: A reveiw. *Applied Catalysis B: Environmental* **2017**, 217, 388-406.

(28) Yue, B.; Li, Q.; Iwai, H.; Kako, T.; Ye, J. Hydrogen production using zinc-doped carbon nitride catalyst irradiated with visible light. *Sci Technol Adv Mater* **2011**, 12, 034401.

(29) Yue, B.; Li, Q.; Iwai, H.; Kako, T.; Ye, J. Hydrogen production using zinc-doped carbon nitride catalyst irradiated with visible light. *Science and Technology of Advanced Materials* **2011**, 12, 034401.

(30) Wang, Y.; Zhou, X.; Xu, W.; Sun, Y.; Wang, T.; Zhang, Y.; Dong, J.; Hou, W.; Wu, N.; Wu, L.; Zhou, B.; Wu, Y.; Du, Y.; Zhong, W. Zn-doped tri-s-triazine crystalline carbon nitrides for efficient hydrogen evolution photocatalysis. *Applied Catalysis A: General* **2019**, 582, 117118.

(31) Xu, J.; Long, K.-Z.; Wang, Y.; Xue, B.; Li, Y.-X. Fast and facile preparation of metal-doped g-C3N4 composites for catalytic synthesis of dimethyl carbonate. *Applied Catalysis A: General* **2015**, 496, 1-8.

(32) Lee, S. C.; Lintang, H. O.; Yuliati, L. A urea precursor to synthesize carbon nitride with mesoporosity for enhanced activity in the photocatalytic removal of phenol. *Chem Asian J* **2012**, 7, 2139-44.

(33) Mu, J.; Li, J.; Zhao, X.; Yang, E.-C.; Zhao, X.-J. Cobalt-doped graphitic carbon nitride with enhanced peroxidase-like activity for wastewater treatment. *RSC Advances* **2016**, 6, 35568-35576.

(34) Sadhukhan, M.; Barman, S. Bottom-up fabrication of two-dimensional carbon nitride and highly sensitive electrochemical sensors for mercuric ions. *Journal of Materials Chemistry A* **2013**, 1, 2752.

(35) Le, S.; Jiang, T.; Zhao, Q.; Liu, X.; Li, Y.; Fang, B.; Gong, M. Cu-doped mesoporous graphitic carbon nitride for enhanced visible-light driven photocatalysis. *RSC Advances* **2016**, 6, 38811-38819.

(36) Wang, N.; Han, Z.; Fan, H.; Ai, S. Copper nanoparticles modified graphitic carbon nitride nanosheets as a peroxidase mimetic for glucose detection. *RSC Advances* **2015**, 5, 91302-91307.

(37) Qiao, F.; Qi, Q.; Wang, Z.; Xu, K.; Ai, S. MnSe-loaded g-C 3 N 4 nanocomposite with synergistic peroxidase-like catalysis: Synthesis and application toward colorimetric biosensing of H 2 O 2 and glucose. *Sensors and Actuators B: Chemical* **2016**, 229, 379-386.

(38) Song, Y.; Qu, K.; Zhao, C.; Ren, J.; Qu, X. Graphene oxide: intrinsic peroxidase catalytic activity and its application to glucose detection. *Adv Mater* **2010**, 22, 2206-10.

(39) Liu, S.; Tian, J.; Wang, L.; Luo, Y.; Sun, X. A general strategy for the production of photoluminescent carbon nitride dots from organic amines and their application as novel peroxidase-like catalysts for colorimetric detection of H2O2and glucose. *RSC Adv.* **2012**, 2, 411-413.

(40) Lu, Q.; Deng, J.; Hou, Y.; Wang, H.; Li, H.; Zhang, Y. One-step electrochemical synthesis of ultrathin graphitic carbon nitride nanosheets and their application to the detection of uric acid. *Chem Commun (Camb)* **2015**, 51, 12251-3.